ACS Photonics

pubs.acs.org/journal/apchd5 Article

Topology of Surface Plasmon Polaritons with Integer and Fractional Orbital Angular Momentum

Published as part of the ACS Photonics virtual special issue " Frontiers and Applications of Plasmonics and Nanophotonics ".

Timothy J. Davis,* Frank J. Meyer zu Heringdorf, and Harald Giessen

Cite This: *ACS Photonics* 2023, 10, 3772–3780 Read Online

ACCESS | Metrics & More | Article Recommendations | Supporting Information

ABSTRACT: The topology of surface plasmon polariton fields (SPPs) with orbital angular momentum (OAM) is characterized by the winding numbers of the phase singularities in the field, also known as topological charges. Using theoretical expressions for the surface plasmon fields, we identify the phase singularities as points where the field is zero and investigate their properties for both integer and noninteger, or fractional, orbital angular momentum. The phase singularities act as vortex centers for the rotating fields. We analyze the behavior of the vortex−antivortex pairs and the breakup of the central vortex and discuss their influence on the measured topology as the orbital angular momentum changes from one integer value l to the next l +1 via the fractional states. Our work highlights the fact that measures of the topological charges do not always equate with the orbital angular momentum and shows how the topology can change discontinuously, even though all of the parameters controlling the fields change smoothly.

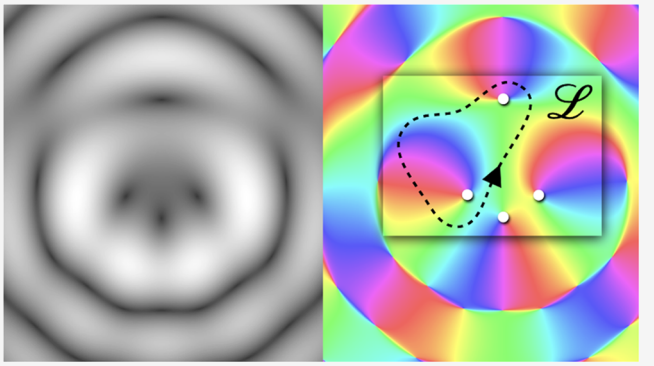

KEYWORDS: *surface plasmon, orbital angular momentum, topology, topological charge, phase singularity*

Downloaded via UNIV OF STUTTGART on January 8, 2024 at 12:10:51 (UTC).
See https://pubs.acs.org/sharingguidelines for options on how to legitimately share published articles.

1. INTRODUCTION

Optical fields with orbital angular momentum may exhibit vortex structures,[1−6] that have been studied for both theoretical interest[7,8] and for potential applications.[9−14] The center of the vortex beam contains a phase singularity where the field amplitude is zero and around which the phase accumulates in multiples l of 2π. This phase singularity is purely topological in nature, and the number of times the phase wraps around the singularity is the topological charge.[15]

Surface plasmon polaritons propagating on metal surfaces can also possess orbital angular momentum, which have been investigated theoretically[16,17] and demonstrated experimentally using near-field scanning optical microscopy.[18,19] More recently, it was shown that the dynamics of surface plasmons with integer orbital angular momentum can be imaged using an optical pump−probe method.[20,21] Excitation of surface plasmons from a spiral boundary results in a plasmon vortex whose dynamics can be reconstructed from a time sequence obtained by adjusting the pump−probe time delay.

The property of integer orbital angular momentum can be extended to fields with noninteger, or fractional, orbital angular momentum, which exhibit a complex structure of phase vortices indicative of a complex underlying topology.[22−25] In this paper, we study the topology of surface plasmon polariton fields (SPPs) with integer and fractional orbital angular momentum (OAM), focusing on the phase singularities in the field that characterize the topology. The phase is a parameter of the field that can be represented in a particular space, such as a point on the unit circle, as we discuss below. Parameter spaces with the same topology can be smoothly and continuously deformed into one another, whereas those with different topology require catastrophic breaking or "surgery" in order to match.[26] Such properties are observed in many physical systems, such as the induced magnetic field from a current in a wire that depends on the topology of two linked curves, one being the magnetic field lines and the other the current loop forming them, as noted by Gauss.[27] In this regard, the shape of the parameter space is less important than its internal connectivity, whereby the singular points, or holes, play an important role.

Received: July 19, 2023
Published: September 26, 2023

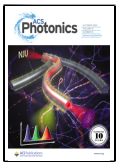

© 2023 American Chemical Society

https://doi.org/10.1021/acsphotonics.3c01024
ACS Photonics 2023, 10, 3772−3780

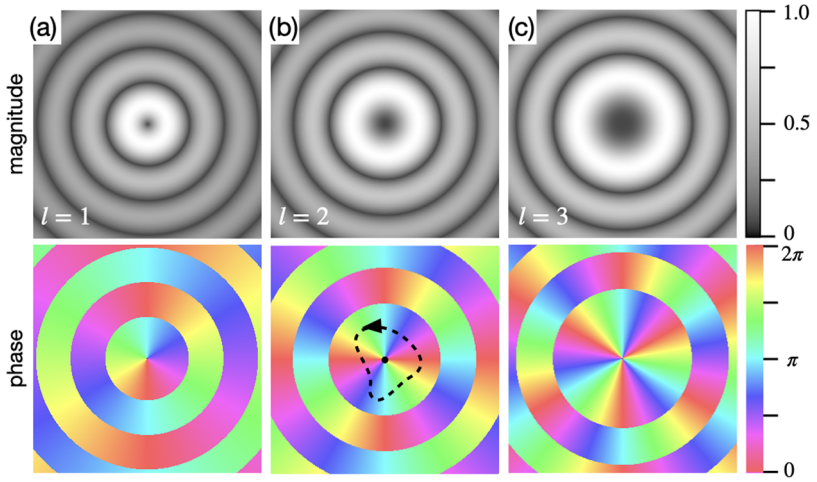

Figure 1. Magnitude and phase profiles of the $\hat{z}$ component of the SPP fields with different integer OAM $L = l$. The magnitude is normalized to 1, and the phase is encoded by the hue. The SPP magnitude is zero at the boundaries across which the phase changes by π. (a) $l = 1$, (b) $l = 2$, and (c) $l = 3$. The dashed line in panel (b) represents a closed path for determining the topology.

These singular points characterize the underlying topology by dividing it into different regions and have a global influence on physical behavior.[26] As such, we examine the regions where the SPP field becomes zero and use techniques of topology to analyze them as the fractional state of the OAM is varied. In particular, we investigate how the topological charge of the SPP fields changes from one integer value to the next, in an apparent discontinuous fashion, even though the OAM changes smoothly through fractional values. We begin with an analysis of SPPs exhibiting integer orbital angular momentum and show how the topology controls the observed behavior of the fields. We then apply this understanding to the situation where the SPPs are excited with noninteger, or fractional, OAM and show how the concepts of topology carry across.

2. RESULTS

2.1. Integer Orbital Angular Momentum. SPPs with orbital angular momentum can be formed on metal surfaces using a variety of techniques.[18,23,25,28] One method involves circularly polarized light incident on a groove etched or milled into the metal surface in the form of an Archimedean spiral,[29,30] with a radius that varies with polar angle ϕ as $R = R_0 + n\phi/\alpha$, where α is the SPP wavenumber. The rotating electric field of the incident light progressively excites SPPs normal to the direction of the groove that propagate toward the center of the spiral, with a phase related to both the radial distance from the spiral center and the phase of the light at the moment of excitation. If the spiral radius increases by an integer n of SPP wavelengths over a full 2π angle, i.e., by $n\lambda_{SPP}$, then all of the waves are excited with well-defined relative phase and develop an orbital angular momentum L characterized by the integer $l = n + s$, where $s = \pm 1$ is the helicity of the incident light. (In the following, we will always represent angular momentum by an integer or a real number. This is equivalent to choosing units where $\hbar = 1$.) Mathematically, the electric field thus created on the surface of the metal can be written in cylindrical coordinates (r, ϕ, z)[31]

$$\chi_l(r, \phi) = e^{il\phi} J_l(\alpha r) \tag{1}$$

with α the wavenumber of the SPP and $J_n(x)$ a Bessel function of the first kind, and we only consider the fields on the surface at $z = 0$. The field has a time dependence $e^{-i\omega t}$ that we do not show. The electric field is then given by

$$\mathbf{E}(r, \phi) = E_0 \alpha \chi_l(r, \phi)\hat{z} + E_0 \frac{\gamma}{\sqrt{2}}[\chi_{l+1}(r, \phi)\hat{e}^- - \chi_{l-1}(r, \phi)\hat{e}^+] \tag{2}$$

The unit vectors $\hat{e}^{\pm} = (\hat{x} \pm i\hat{y})/\sqrt{2}$ are associated with left and right rotations and E_0 is an amplitude. For SPPs excited on thick metal films by light of frequency ω or wavenumber $k = \omega/c$, the in-plane SPP wavenumber is[32,33]

$$\alpha = k\sqrt{\frac{\epsilon_m \epsilon_b}{\epsilon_m + \epsilon_b}} \tag{3}$$

and $\gamma^2 = \alpha^2 - \epsilon_b k^2$ with metal relative permittivity ϵ_m adjacent to a dielectric of relative permittivity ϵ_b. In eq 2, we observe that the electric field naturally divides into three terms with different OAM, as indicated by the terms χ_l and $\chi_{l\pm1}$. That the in-plane field components express different OAM states is due to a geometric phase term arising from the change in orientation of the boundary normal with position. For simplicity, we consider only the $\hat{z}$ field components normal to the surface although all considerations apply to the other components.

Figure 1 shows the magnitude of the normal component of the SPP field and the phase for three different OAM, calculated using eq 1. The SPPs propagating from the boundary and interfering produce a phase structure equivalent to an optical vortex.[20,34] For $l > 0$, the characteristic features of SPP fields are as follows: they become zero at the center of the spiral and have a phase that changes by $2\pi l$ as we follow a closed path around the central zero. At this zero point, the phase is undefined, which represents a singularity in the phase parameter space. We also observe that the field becomes zero in rings at certain radii across which the phase changes abruptly by π.

The field of topology is concerned with the properties that remain fixed under smooth deformations of the underlying geometry. One of the methods for identifying the topology of a particular space in two dimensions is to consider closed loops (or surfaces and hyper surfaces in higher dimensions) and how these can be translated and deformed over the surface.[26,35] A

https://doi.org/10.1021/acsphotonics.3c01024
ACS Photonics 2023, 10, 3772−3780

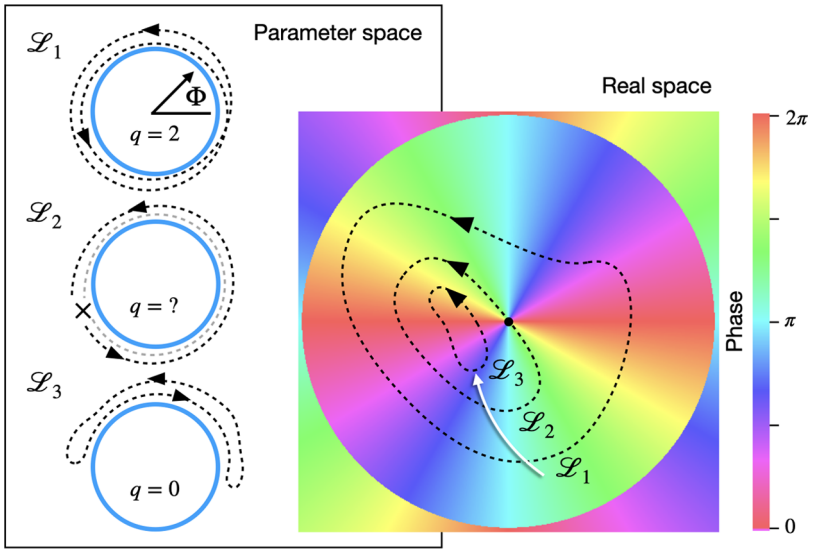

Figure 2. Three directed contours ($\mathcal{L}_1$, $\mathcal{L}_2$, $\mathcal{L}_3$) in the plane of the SPP field, with $l = 2$, mapping the phase onto unit circles (shown in blue) of the parameter space. The dashed lines around the blue circles represent the paths in parameter space, all three of which are topologically distinct. Loop $\mathcal{L}_1$ spans one loop in real space but maps to two connected loops in phase space. Contour $\mathcal{L}_2$ passes through the singular point, which appears as a broken path marked by ×. The white arrow in the real space represents how the contours might be transformed into one another.

typical example of two different topologies is those of a sphere and a torus. It is impossible to smoothly deform a sphere into a torus without breaking it. Moreover, any closed loop on the surface of the sphere can be deformed into a point, whereas a closed loop that runs around the edge of a torus cannot. The center "hole" in the torus acts like a singularity that prevents a continuous smooth deformation.

In the following, we study the topology of the space that represents the phase Φ of the SPP field. Parameters in this space are represented by points on the unit circle, where the phase maps onto the polar angle that locates the point. The phase can also be represented by a complex number $z = e^{i\Phi} = e^{il\phi}$, as evident from eq 1, or equivalently by a unit vector $\hat{v} = \hat{x}\cos\Phi + \hat{y}\sin\Phi$ with a direction determined by the phase. As we traverse a path in real space, we map each phase there onto the unit circle, i.e., map the phase from real space onto its parameter space. It is the topology of the resulting path in the parameter space that is important.

2.1.1. Phase Singularity. At the center of the SPP wave field, there is a phase singularity, sometimes referred to as a vortex. The phase singularity can be thought of as a defect in the parameter space[26] because the value at this point is undefined and therefore is not an element of the parameter space. A contour in real space around the singularity maps onto the unit circle in parameter space, and it covers this space l times. The phase on this circle is an element of the two-dimensional (2D) proper rotation group SO(2). An example is shown by contour $\mathcal{L}_1$ in Figure 2. Translations or distortions of the contour in real space (represented by the white arrow in Figure 2) do not change the loop in parameter space until the contour crosses the singularity. At that point, the mapping breaks down ($\mathcal{L}_2$), and the continuous loop in parameter space breaks at a point. Once the singularity is no longer encircled by the contour, the loop in parameter space winds back on itself ($\mathcal{L}_3$).

The two contours $\mathcal{L}_1$ and $\mathcal{L}_3$ in parameter space are not homotopic in that they have different topologies. This is obvious from the fact that they wind around the parameter space a different number of times. The topology of the field in the vicinity of the singularity is characterized by this winding number (also referred to as the topological charge or vorticity), which measures the number of times the path loops around the parameter space (e.g., twice for $\mathcal{L}_1$ and zero for $\mathcal{L}_3$). The winding number can be obtained from a mapping from the path in real space to that in parameter space by integrating the phase gradient around the singularity

$$q = \frac{1}{2\pi}\oint \frac{\partial\Phi}{\partial\rho}\mathrm{d}\rho \tag{4}$$

This integral will yield the integer value for the orbital angular momentum of the SPP field. For example, the phase of the normal component of the SPP with integer OAM $L = l$ close to $r = 0$ is $\Phi = l\phi$, as in eq 1. Writing $\rho \equiv \phi$, then trivially $\partial\Phi/\partial\phi = l$, and the integral over 2π results in $q = l$. In this way, the OAM of the SPP field is synonymous with the topological charge of the phase singularity, and therefore, SPP fields with different OAM are topologically distinct. From this observation, we note that the three electric field components in eq 2 in directions $\hat{z}$, $\hat{e}^+$, and $\hat{e}^-$ are also topologically distinct because they are associated with different OAM integers l and therefore different topological charges or winding numbers.

Before we leave this section, it is useful to introduce the concept of combining paths in real space. Two adjacent paths can be joined by a smooth transformation that brings one or more points on one path into contact with another, thereby allowing both paths to be traversed in turn. Such an operation results in paths having a group structure.[26,35] Furthermore, the winding numbers associated with each path then simply add together. We use this property when considering singularities created by fractional OAM.

2.1.2. Phase Rings. In the SPP OAM fields, we observe rings where the field is zero and across which the phase changes by π. These are located at radii where the Bessel function in eq 1 passes through zero, $J_l(\alpha r) = 0$. On such rings (which we refer to as "phase rings"), the phase is again undefined. Unlike the singular points at the center of the

https://doi.org/10.1021/acsphotonics.3c01024
ACS Photonics 2023, 10, 3772−3780

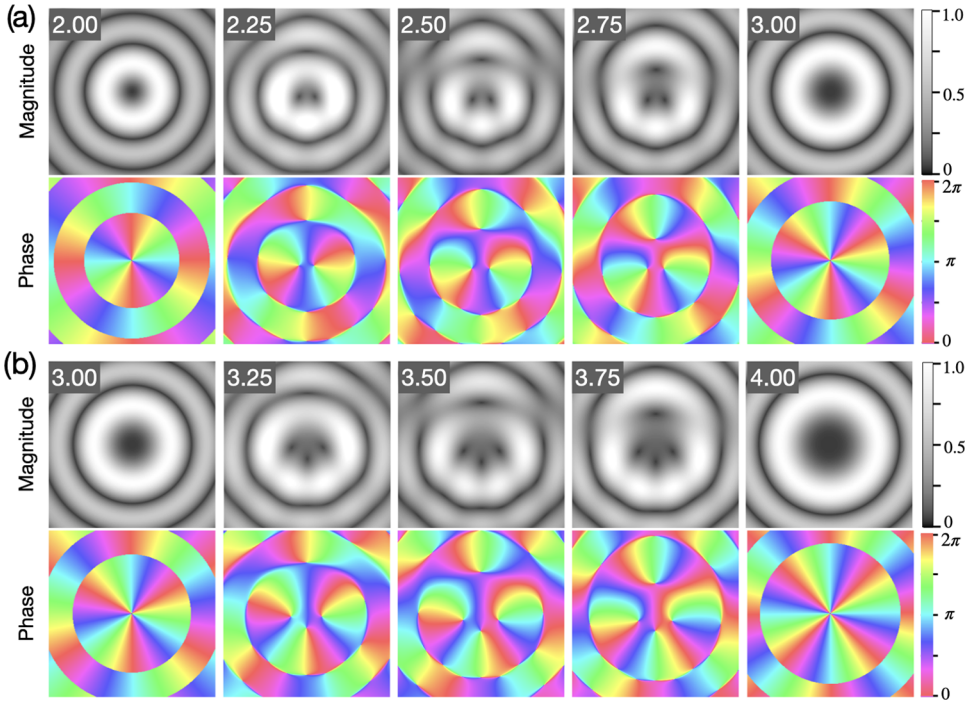

Figure 3. SPP field magnitude and phase as the parameter controlling the gap in the Archimedean spiral increases from (a) $\nu = 2$ to $\nu = 3$ and (b) $\nu = 3$ to $\nu = 4$.

vortex, these phase rings are topologically trivial in that they do not influence the topology of the parameter space. To see this, consider two loops encompassing the central vortex: one loop just inside a phase ring and another just outside it. It is obvious that integrating the phase change around each loop yields the same winding number $q = l$, proving that the phase ring has no influence on the topology and that the phase ring itself has zero topological charge $q_{pr} = 0$. When we study fractional OAM, we will find that the phase ring breaks up into an equal number of phase singularities such that the total topological charge remains zero.

2.1.3. Central Zero-Field Region. The last feature of interest in the SPP field with integer OAM is the region close to the center where the field magnitudes are very small. The size of this region increases with increasing l, as observed in Figure 1. This property has a simple explanation in terms of the SPP wavelength $\lambda_{spp} = 2\pi/\alpha$. The SPP field with integer OAM $L = l$ consists of a wave with l wavelengths in a circle about the origin. This wave can exist only in a region of critical radius r_c such that the distance around the circle is equal to the number of wavelengths $2\pi r_c = l\lambda_{spp}$ or $\alpha r_c = l$. As the radius $r \ll r_c$ becomes much smaller than r_c, it becomes increasingly difficult to compress l waves around the circle, resulting in wave crests and troughs overlapping, causing the field strength to weaken and eventually become zero. Such behavior is characterized by the Bessel function $J_l(\alpha r)$ that has a value significant only when $\alpha r \approx l$, and it reaches its first maximum after $\alpha r > l$. This property is also important when considering the fracturing of the phase ring with noninteger OAM.

2.2. Fractional OAM. Surface plasmon polaritons with noninteger, or fractional, OAM can be created by modifying the gap in the Archimedean spiral to have a length equal to a noninteger $\nu - s$ number of wavelengths.[29] Under this condition, eq 1 can be generalized following the method of Berry,[7] which takes the form of an infinite series (derived in the Supporting Information)

$$\mathcal{A}_\nu(r, \phi') = \sum_{n=-\infty}^{\infty} a_n(\nu) e^{in\phi'} J_n(\alpha r) \tag{5}$$

where

$$a_n(\nu) = \frac{e^{i\nu\pi} \sin \nu\pi}{\pi(\nu - n)} \tag{6}$$

In this equation, we have rotated the coordinate system so that $\phi' = \phi - \pi/2$, which removes a factor $(-i)^n$ from the definition of $a_n(\nu)$. That the wave field can be expressed as a series of integer OAM states is not unexpected, but this also has its origin in topology. Only those wave components with phases that change about the origin by an integer number of 2π can exist, which is expressed exactly in the series in eq 5. Such a decomposition has been observed recently in time-resolved experiments of SPPs with fractional OAM.[36] The vector electric field of the SPP on the metal surface at $z = 0$ takes the form

$$\mathbf{E}(r, \phi', z) = E_0 \alpha \mathcal{A}_\nu(r, \phi')\hat{z} + E_0 \frac{i\gamma}{\sqrt{2}} [\mathcal{A}_{\nu+1}(r, \phi')\hat{e}^- + \mathcal{A}_{\nu-1}(r, \phi')\hat{e}^+] \tag{7}$$

in direct analogy with eq 2. For $\nu = l$, an integer, it can be shown using a limiting process that $\sin l\pi / (l - n)$ is nonzero only when $n = l$, giving $a_l(l) = 1$ and $a_{n\neq l}(l) = 0$, which leaves the nonzero term as the Bessel function and phase $\mathcal{A}_l(r, \phi') = \chi_l(r, \phi') = e^{il\phi'} J_l(\alpha r)$ as before.

The representation of $\mathcal{A}_\nu(r, \phi')$ in eq 5 is a linear combination of integer angular momentum functions with

https://doi.org/10.1021/acsphotonics.3c01024
ACS Photonics 2023, 10, 3772−3780

expansion coefficients $a_n(\nu)$. These expansion coefficients are normalized such that

$$\sum_{n=-\infty}^{+\infty} |a_n(\nu)|^2 = \frac{\sin^2 \nu\pi}{\pi^2} \sum_{n=-\infty}^{\infty} \frac{1}{(\nu - n)^2} = 1 \tag{8}$$

since $\sum_n (\nu - n)^{-2} = \pi^2/\sin^2 \pi\nu$ is a series representation of $\pi^2 \operatorname{cosec}^2 \pi\nu$. Therefore, we can think of the expansion coefficient $a_n(\nu)$ as the probability amplitude to find a surface plasmon with integer angular momentum n. The coefficient also obeys the useful relation $a_n(\nu \pm 1) = a_{n\mp1}(\nu)$.

The relationship between the Archimedean spiral parameter ν and the orbital angular momentum can be derived by applying the angular momentum operator $\hat{L} = -i\,\partial/\partial\phi$ to each field component, as discussed in the Supporting Information. The result is

$$L = \sum_{n=-\infty}^{\infty} n\,|a_n(\nu)|^2 = \nu - \frac{\sin 2\pi\nu}{2\pi} \tag{9}$$

where we have included an intermediate result showing that the total fractional OAM is just the sum of the integer angular momentum n of each individual state weighted by the probability $|a_n(\nu)|^2$ that they are excited. This relation has been verified for SPPs in experiments[36] and is the same for optical beams with fractional OAM, which has also been measured experimentally.[37] When $\nu = l$ is an integer, this equation reduces to the result for the integer OAM as required.

The behavior of the SPP field with changing fraction ν is complicated.[23] For simplicity, we consider only the $\hat{z}$ component of the SPP field as the other two components display similar behavior. The magnitude and phase of $A_\nu(r, \phi')$ in the plane of the metal are shown in Figure 3 as the gap in the Archimedean spiral $(\nu - s)\,\lambda_{spp}$, characterized by ν, changes from $\nu = 2$ to $\nu = 4$. We observe the splitting of the central vortex into individual vortices, the breakup of the phase ring into vortex−antivortex pairs (where an antivortex is defined as a vortex with negative topological charge) with one of the vortices tracking down from the phase ring toward the center where it finally combines with the other central vortices. This behavior is most clearly observed in a movie simulation, available online for $0 \le \nu < 6.1$. In the following we consider these behaviors individually.

2.2.1. Splitting of Central Phase Singularity. For integer OAM $\nu = l$, a single phase vortex with topological charge $q = l$ exists at the center of the Archimedean spiral. This phase singularity is unstable in that a small perturbation to the field will cause it to split into l individual singularities, as observed in optical beams.[15,38] This splitting behavior can be demonstrated using complex numbers to represent the field at each point in the plane close to the origin. Let $z = r\,e^{i\phi}$, so that a field ψ with a singularity of topological charge l at the origin is given by $\psi = z^l$. In the presence of a small field offset $z_0 = |z_0|e^{i\phi_0}$, where now $\psi = z^l - z_0$, the phase singularities shift to new positions $z = z_0^{1/l}$ or at a distance from the origin $|z_0|^{1/l}$ and at angles $\phi = \phi_0/l + 2\pi n/l$, where $0 \le n < l$. Thus, we have shown that a phase singularity will split into l singularities with topological charges $q = 1$. In this regard, it is the sum of the topological charges near the center of the spiral that equates to the OAM number l.

Likewise, as ν increases away from the integer value $\nu > l$, the central phase singularity splits into l individual singularities, which is also due to the presence of additional fields, as we now demonstrate. These additional fields arise from the sequence of integer OAM states that are mixed into the OAM state l, as shown in the sum in eq 5. We estimate the effect of these fields by considering a region close to the origin so that $\alpha r \ll 1$. Here, the Bessel function $J_n(\alpha r) \approx (\alpha r)^n/2^n\,n!$. We also let $\nu = l + \delta\nu$ deviate from an integer l by a small amount $\delta\nu$, which enables us to approximate the SPP field by

$$A_\nu(r, \phi') \approx \delta\nu e^{i\delta\nu\pi} \sum_{n=-\infty}^{\infty} \frac{z^n}{2^n n!(l - n + \delta\nu)} \tag{10}$$

where $z = \alpha r\, e^{i\phi'}$. Only three terms in this sum dominate for small values $\delta\nu$. The denominator varies with $2^n\,n!$ so that the first two terms $n = 0$ and $n = 1$ are significant. Likewise, the denominator term $(l - n + \delta\nu)$ is small when $n = l$. Thus, in this approximation, the field with OAM $L = l$, represented by z^l, is perturbed by a background field z^0 with no OAM and a field z^1 with OAM $L = 1$. The phase singularities occur where $A_\nu(r, \phi') = 0$ or equivalently where $z^l + v_1\,z + v_0 = 0$ with $v_n = 2^{l-n}\,l\,!\,\delta\nu/(\nu - n)$. Since this is a polynomial of order l, it has at most l roots or zeros, which is consistent with the total topological charge. To see how the vortices are arranged about the origin, we let $z = z_0 + \delta z$, where z_0 satisfies $z_0^l + v_0 = 0$, and then writing $(z_0 + \delta z)^l \approx z_0^l + l\,z_0^{l-1}\delta z$ gives an approximate solution

$$z_m \approx \frac{l v_0}{l v_0^{(l-1)/l} e^{i\pi(1+2m)/l} - v_1} \tag{11}$$

There are l complex solutions, each labeled by an integer m where $0 \le m < l$, that locate the topological charges near the center of the vortex.

Our analysis shows that the total topological charge in this region remains constant for small $\delta\nu$ and implies that the single charge at the center is a sum of l individual charges. The locations of the topological charges calculated by using eq 11 are compared with a full numerical solution of eq 5 in Figure 4, which shows reasonable agreement, given the simplifications employed. Thus, we find that the topology associated with a small region that encompasses all of these central points remains the same as before. A line integral around such a region will again yield a winding number l and a topological charge $q = l$, although this property breaks down as $\nu \to l + 1$

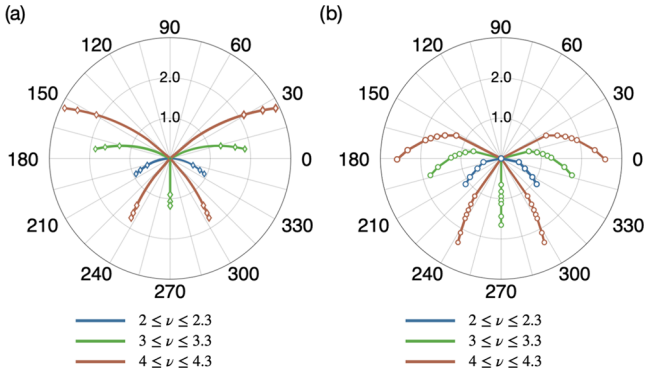

Figure 4. Polar plots of the trajectories of the central vortices as ν varies over three different ranges: $2 \le \nu \le 2.3$, blue curves; $3 \le \nu \le 3.3$, green curves; and $4 \le \nu \le 4.3$, red curves. (a) Calculation using eq 11. The open diamonds points mark fractional values $\nu - l = 0.1$, 0.2, and 0.3 with 0.0 at the origin. (b) Exact numerical solution of $\mathcal{A}_\nu(\alpha r, \phi') = 0$ with circles marking the calculated points. The solid lines are guides for the eye. The rings mark the radii in units of αr.

https://doi.org/10.1021/acsphotonics.3c01024
ACS Photonics 2023, 10, 3772−3780

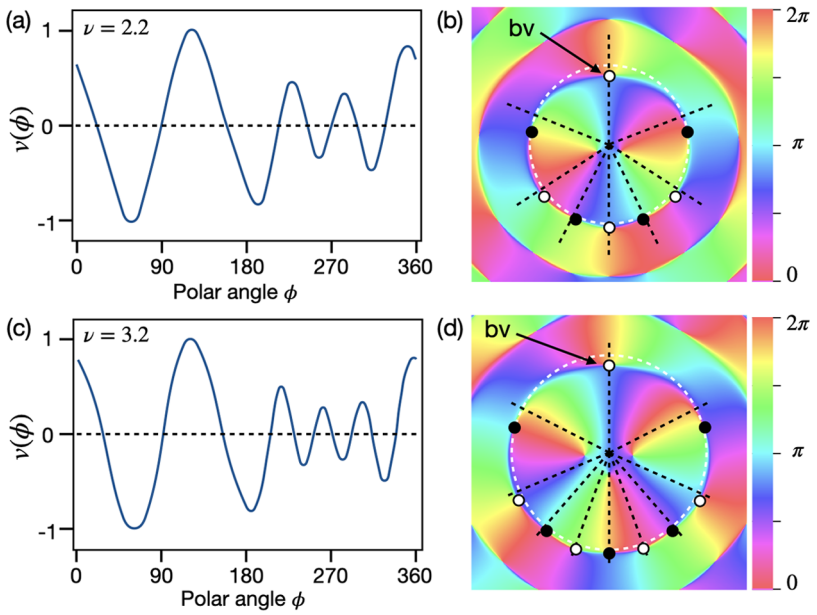

Figure 5. Angles at which the phase vortices appear on the first phase ring. (a) The graph of $\nu(\phi)$ based on eq 15 for $\nu = 2.2$. The zero-crossings locate the angles at which the vortices lie. (b) Calculation of the relative phase distribution for SPPs associated with $\nu = 2.2$. The white/black dots locate the phase singularities with topological charge +1/−1 respectively. The dashed radial lines are at the angles associated with the zero-crossings in panel (a) and the white dotted circle shows the location of the phase ring where $J_2(\rho_0) = 0$. The vortex labeled "bv" is the "birth vortex" that tracks down to the center of the field increasing the topological charge there by 1. (c, d) Corresponding curves and phase distributions for $\nu = 3.2$ with the white dotted circle locating the phase ring where $J_3(\rho_0) = 0$.

as we show below. Importantly, we find that the combined topological charge $q = l$ in this region is no longer equal to the OAM of the field, which now has the fractional value given by eq 9. This implies that simply counting the winding number of the phase about some region is not a good measure of the OAM, except in some cases for integer values.

The above analysis also suggests that the locations of the central vortices do not determine the fractional angular momentum of the field. From eq 9, we note that the field component with zero OAM, with an amplitude a_0, does not contribute to the fractional angular momentum since $n = 0$. This implies that an additional field with zero OAM can be added to the existing fields with no effect on the OAM. Moreover, as we have shown, the presence of an additional field causes the phase singularities to move apart, which suggests that the fractional OAM is independent of the positions of the central vortices, at least on the order of approximations we have used.

2.2.2. Breakup of the Phase Ring. A key feature of the transition from integer to noninteger orbital angular momentum is the disruption of the phase rings. For the integer OAM, these rings occur where the Bessel function $J_l(\alpha r)$ passes through zero and changes sign. The sign change creates a phase flip across the phase ring. As discussed above, the rings themselves carry no topological charge. However, for a small deviation from integer $\delta\nu = \nu - l$, the phase ring breaks into $2(l + 2)$ individual vortices with alternating topological charge such that they sum to zero. As we will show, the number of vortices is determined by the number of OAM harmonics that can exist in the location of the phase ring, which depends on the OAM integer l and the wavelength of the SPP, which in turn determine the size of the "dark" region of the SPP field magnitude about the center.

We estimate the locations of the vortices that form from the phase ring with increasing ν using an approximation to $\mathcal{A}_\nu(r, \phi')$ in the vicinity of the phase ring. For the integer OAM, the ring is located at ρ_0 where $J_l(\rho_0) = 0$. We let $\nu = l + \delta\nu$ be close to the integer value l, where $\delta\nu \ll 1$ as before. The wave function is then approximately

$$\mathcal{A}_\nu(\rho, \phi') \approx \delta\nu e^{il\phi' + i\delta\nu\pi} \sum_{m=-\infty}^{\infty} \frac{1}{(\delta\nu - m)} e^{im\phi'} J_{l+m}(\rho) \tag{12}$$

where m is the integer deviation from l. The change in each Bessel function around the point ρ_0 where $J_l(\rho_0) = 0$ can be written to first order as $J_n(\rho_0) + (dJ_n(x)/dx)|_{\rho_0}\, \delta\rho$, which combined with a standard relation between the derivatives of Bessel functions, leads to

$$\mathcal{A}_\nu(\rho, \phi') \approx e^{i(l+\delta\nu)\pi} \sum_{m=-\infty}^{\infty} e^{im\phi'} J_{l+m}(\rho_0) \left(\frac{\delta\nu}{\delta\nu - m} + \frac{\delta\rho}{2} \left[\frac{e^{i\phi'}}{\delta\nu - m - 1} - \frac{e^{-i\phi'}}{\delta\nu - m + 1} \right] \right) \tag{13}$$

By definition, the term with $m = 0$ is zero because $J_l(\rho_0) = 0$. We treat $\delta\nu$ and $\delta\rho$ as small, neglect all terms second order and above in small quantities, and approximate $\delta\nu - m \approx -m$. However, the terms with $m = \pm 1$ must be treated separately because the denominators cancel $\delta\nu$ in the numerator. Using the relation between Bessel functions $J_{l-1}(\rho_0) = (2l/\rho_0) J_l(\rho_0) - J_{l+1}(\rho_0) = -J_{l+1}(\rho_0)$, where $J_l(\rho_0) = 0$, combining terms together, and noting that the phase singularities are located where $\mathcal{A}_\nu(\rho_0 + \delta\rho, \phi') = 0$, we obtain

https://doi.org/10.1021/acsphotonics.3c01024
ACS Photonics 2023, 10, 3772−3780

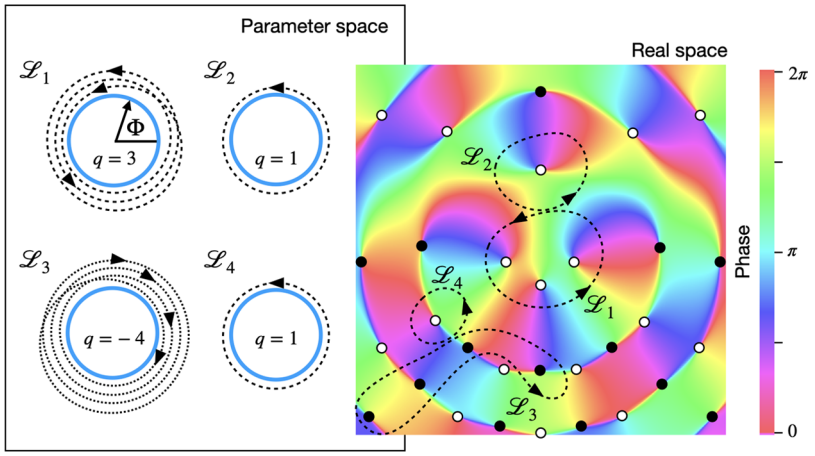

Figure 6. SPP phase distribution Φ for $\nu = 3.5$ showing the complex distribution of vortices (white dots) and antivortices (black dots) and the topology of the parameter space associated with four different paths in real space. The number of loops in parameter space corresponds to the total topological charge contained by the loop: $q = 4$ for $\mathcal{L}_1$, $q = 1$ for $\mathcal{L}_2$ and $\mathcal{L}_4$, and $q = -4$ for $\mathcal{L}_3$ since the sense of rotation in phase space is opposite.

$$\delta\rho \approx -2\delta\nu\cos\phi' + \delta\nu \sum_{m=2}^{\infty} \frac{J_{l-m}(\rho_0)e^{-im\phi'} - J_{l+m}(\rho_0)e^{im\phi'}}{mJ_{l+1}(\rho_0)} \tag{14}$$

Since the position $\delta\rho$ must be real, we require the imaginary terms in eq 14 to sum to zero. This yields an expression that is zero at the angles where the phase ring breaks into phase vortices

$$\nu(\phi') = \sum_{m=2}^{\infty} \sin m\phi' \left\{ \frac{J_{l-m}(\rho_0) + J_{l+m}(\rho_0)}{mJ_{l+1}(\rho_0)} \right\} = 0 \tag{15}$$

It is clear that there will always be vortices at $\phi' = 0$ and at $\phi' = \pi$ as these angles always satisfy eq 15. As we discussed previously, the topology of the space and the requirement for phase continuity means that Bessel functions $J_n(\rho_0)$ contribute to the sum in eq 15 only while the index n is less than $n < \rho_0 \sim l + 1$. Because the term $J_{l-m}(\rho_0)$ depends on $l - m$, this requires m to be summed to at least $2(l + 1)$ after which the OAM states contribute little to the sum. The points where $\nu(\phi')$ is zero determine the vortex locations. This function is independent of $\delta\nu$, and thus, we expect the vortices to remain approximately at the same angular positions as ν is varied.

Examples of calculations of the locations of vortices breaking from the phase ring are shown in Figure 5 for $\nu = 2.2$ and $\nu = 3.2$. Again, despite the approximations employed, the angles at which $\nu(\phi) = 0$ correspond closely to the positions of the vortices calculated using eq 5. Moreover, from eq 14, we expect the vortices to lie inside the original phase ring for $-\pi/2 < \phi' < \pi/2$, or $0 < \phi < \pi$, where $\delta\rho$ is negative, and outside otherwise, which is in reasonable agreement with the locations shown in Figure 5. The expression finds the precise number of phase singularities as $N_s = 2(l + 2)$, where $\nu = l + \delta\nu$.

Note that the sign of the winding number of each vortex is given by the sign of the gradient $d\nu(\phi')/d\phi'$ because this determines the phase change across the vortex relative to the previous vortex. Again, for purely topological reasons, the curve can only pass through zero by alternating negative-to-positive $(d\nu/d\phi' > 0)$ and positive-to-negative $(d\nu/d\phi' < 0)$ transitions, thus enforcing the vortices to have topological charges following an alternating $+q$ and $-q$ pattern, as we observe.

2.2.3. Birth Vortex. The "birth vortex" is the phase singularity that appears at $\phi = \pi/2$ on the phase ring and slowly tracks down to the origin as ν varies from one integer l to the next $l + 1$ (see, e.g., Figure 5 and the movie in the Supporting Information). The properties of such vortices were observed in optical fields with fractional OAM.[39] Unlike the other vortices created at the phase ring that eventually dissolve into a new phase ring, this vortex remains and combines with those at the center to increase the topological charge by one. This would leave the phase ring with a charge of -1 except that another vortex of topological charge $q = 1$ breaks away from the next outer phase ring and joins the inner one, thereby balancing the topological charge. This mechanism is repeated for all phase rings, effectively out to infinity, as observed in optical fields.[7,22] This process leaves all phase rings with zero net topological charge except at the center of the field where the charge increases by $q = 1$. This mechanism for fractional vortices is a physical example of Hilbert's hotel paradox.[40]

The approximate location of this singularity is obtained from the real part of eq 14 with $\phi = \pi/2$ or $\phi' = 0$,

$$\rho \approx \rho_0 - \delta\nu\left(2 + \sum_{m=2}^{\infty} \frac{J_{l+m}(\rho_0) - J_{l-m}(\rho_0)}{mJ_{l+1}(\rho_0)}\right) \tag{16}$$

From this expression, we see that the "birth vortex" begins at the phase ring at $\alpha r = \rho_0$ when $\nu = l$, and because of the minus sign $-\delta\nu$, it then moves toward the center as $\nu \to l + 1$. From the point of view of the topology of the SPP phase, a loop enclosing the l central vortices maps the phases over the parameter space l times. Eventually, however, the birth vortex crosses the loop causing the mapping to parameter space to fail, just as with $\mathcal{L}_2$ in Figure 2, after which the path in parameter space is covered $l + 1$ times, as would be expected for OAM $l + 1$.

2.2.4. Topology of Fractional OAM. The local topology of the parameter space for fractional OAM is complicated because of the distribution of topological charges with both positive and negative winding numbers. The phase change along a loop and therefore the topological charge contained within the loop depend on the particular path taken in real

https://doi.org/10.1021/acsphotonics.3c01024
ACS Photonics 2023, 10, 3772−3780

space, as exemplified in Figure 6. Paths that encompass antivortices, as with $\mathcal{L}_3$ in Figure 6, result in loops in parameter space that run clockwise, represented by a negative winding number. Combining paths together yields a sum of winding numbers, as is evident with $\mathcal{L}_1$ and $\mathcal{L}_2$ in Figure 6. One can follow path $\mathcal{L}_1$ to the point where it coincides with $\mathcal{L}_2$, then follow path $\mathcal{L}_2$ until it coincides again with $\mathcal{L}_1$, and then complete the loop back to the starting position. This process results in $q = 3 + 1 = 4$. Likewise, combining $\mathcal{L}_3$ and $\mathcal{L}_4$ leads to an enclosed topological charge $q = -4 + 1 = -3$.

It is possible to choose a path in real space to obtain any topological charge between $-\infty < q < +\infty$ because the pattern of vortex−antivortex pairs continues to infinity. This is perhaps unsurprising because the SPP field contains all possible OAM states, as shown in eq 6. As we discussed above, the fractional OAM seems not to depend on the location of the central vortices and the fact that paths can be chosen to sample any winding number provides further evidence to support the notion that the value of the fractional orbital angular momentum has no relation to the locations and number of the phase singularities.

We are in a position to answer the question regarding how the topological charge can increase discontinuously by 1, i.e., $l \rightarrow l + 1$, when the spiral parameter ν changes smoothly from $\nu = l$ to $\nu = l + 1$. For any sufficiently large path near the center of the spiral that always contains the central vortices (e.g., $\mathcal{L}_1$), the topological charge is $q = l$ until the birth vortex crosses the path and changes the measured parameter space topology. This will always occur because all central vortices eventually move inward to the center of the spiral, including the birth vortex, where they all combine into one singularity. Thus, the birth vortex will always cross any such path, and the topological charge about the center will change discontinuously. In addition, as $\nu \rightarrow l + 1$, the vortex−antivortex pairs from the phase rings stretch azimuthally and recombine to form a new phase ring with a net-zero topological charge, located at ρ_0 such that $J_{l+1}(\rho_0) = 0$.

3. DISCUSSION

The presence of many vortex−antivortex pairs for fractional OAM indicates a complex fractured topology for the SPP field, which has no definite global winding number, as it depends on the path taken in real space. Therefore, although all parameters in the SPP field change smoothly with ν, the measure of the topology within a region always changes discontinuously. Such behavior of SPP fields with fractional OAM has been observed in experimental realizations of SPP fields[36] using a variety of methods such as aperture-based phase- and polarization-resolved near-field scanning optical microscopy (NSOM)[41−43] and time-resolved methods such as optical pump−probe two-photon photoemission electron microscopy (2PPE−PEEM).[20,21,31]

Given the complex nature of SPP fields exhibiting fractional OAM, we may have foreseen that there would be no direct correspondence between fractional OAM and the topological charge. However, more surprising is that the absence of a direct correspondence between OAM and the topological charge can occur in fields with integer OAM. Using a mathematical description of optical fields in the paraxial approximation, Berry and Lie[44] recently showed that it is possible for scalar fields to possess integer OAM but contain zero topological charge, as well as scalar fields with zero OAM having nonzero topological charge. Such theoretical observations present a challenge in demonstrating these effects experimentally.

4. CONCLUSIONS

In this work, we have applied methods of algebraic topology to investigate the phase singularities that are found in surface plasmon polariton fields exhibiting orbital angular momentum, as would be created by excitation at the boundary of an Archimedean spiral. For SPP fields exhibiting integer OAM, we note the presence of a phase vortex with a phase singularity at its center that has a topological charge directly related to the angular momentum of the field. As implied by Berry and Lie, this is a fortuitous occurrence and such a relationship may not occur for all SPP fields with integer OAM. For SPP fields with fractional OAM, we find that there are an infinite number of phase singularities and we studied the properties of the central-most ones as the Archimedean spiral gap parameter ν increases. We find that there is no relationship between the topological charges and the fractional value of the OAM. Our work shows that using topological charge as a measure of orbital angular momentum is not always valid.

■ ASSOCIATED CONTENT

Supporting Information

The following files are available free of charge. The Supporting Information is available free of charge at https://pubs.acs.org/doi/10.1021/acsphotonics.3c01024.

Mathematical derivations (PDF)

Video showing the central and birth phase singularities as functions of the fractional OAM parameter ν (MP4)

■ AUTHOR INFORMATION

Corresponding Author

Timothy J. Davis − *University of Melbourne, School of Physics, Parkville, Victoria 3010, Australia;* orcid.org/0000-0002-7299-4900; Email: timd@unimlb.edu.au

Authors

Frank J. Meyer zu Heringdorf − *University of Duisburg-Essen, Faculty of Physics and Center for Nanointegration (CENIDE), 47048 Duisburg, Germany;* orcid.org/0000-0002-5878-2012

Harald Giessen − *University of Stuttgart, 4-th Physics Institute and Research Center SCoPE, 70569 Stuttgart, Germany*

Complete contact information is available at: https://pubs.acs.org/10.1021/acsphotonics.3c01024

Funding

This work was funded by the Deutsche Forschungsgemeinschaft (DFG, German Research Foundation) SFB 1242 Project Nos. 278162697, SPP1391 Ultrafast Nanooptics, and GRK2642 Photonic Quantum Engineers; the European Research Council (ERC) projects Complexplas and 3DPrinteoptics; a Baden-Württemberg Stiftung Spitzenforschung Opterial; the German Federal Ministry of Education and Research BMBF project Printoptics; and Carl-Zeiss Stiftung. T.J.D. acknowledges support from the Max Planck Institute (MPI) Guest Professorship Program and from the DFG (GRK2642) Photonic Quantum Engineers for a Mercator Fellowship.

Notes

The authors declare no competing financial interest.

REFERENCES

(1) Coullet, P.; Gil, L.; Rocca, F. Optical vortices. *Opt. Commun.* **1989**, *73*, 403−408.
(2) Allen, L.; Beijersbergen, M. W.; Spreeuw, R. J. C.; Woerdman, J. P. Orbital angular momentum of light and the transformation of Laguerre-Gaussian laser modes. *Phys. Rev. A* **1992**, *45*, 8185−8189.
(3) Heckenberg, N. R.; McDuff, R.; Smith, C. P.; Rubinsztein-Dunlop, H.; Wegener, M. J. Laser beams with phase singularities. *Opt. Quantum Electron.* **1992**, *24*, S951−S962.
(4) Bazhenov, V. Y.; Soskin, M. S.; Vasnetsov, M. V. Screw Dislocations in Light Wavefronts. *J. Mod. Opt.* **1992**, *39*, 985−990.
(5) David, A.; Gjonaj, B.; Bartal, G. Two-dimensional optical nanovortices at visible light. *Phys. Rev. B* **2016**, *93*, No. 121302.
(6) Shen, Y.; Wang, X.; Xie, Z.; Min, C.; Fu, X.; Liu, Q.; Gong, M.; Yuan, X. Optical vortices 30 years on: OAM manipulation from topological charge to multiple singularities. *Light: Sci. Appl.* **2019**, *8*, No. 90.
(7) Berry, M. V. Optical vortices evolving from helicoidal integer and fractional phase steps. *J. Opt. A: Pure Appl. Opt.* **2004**, *6*, 259−268.
(8) Dennis, M. R.; King, R. P.; Jack, B.; O'Holleran, K.; Padgett, M. J. Isolated optical vortex knots. *Nat. Phys.* **2010**, *6*, 118−121.
(9) Wang, W.; Yokozeki, T.; Ishijima, R.; Wada, A.; Miyamoto, Y.; Takeda, M.; Hanson, S. G. Optical vortex metrology for nanometric speckle displacement measurement. *Opt. Express* **2006**, *14*, 120−127.
(10) Yao, A. M.; Padgett, M. J. Orbital angular momentum: origins, behavior and applications. *Adv. Opt. Photonics* **2011**, *3*, 161−204.
(11) Padgett, M. J. Orbital angular momentum 25 years on [Invited]. *Opt. Express* **2017**, *25*, 11265−11274.
(12) Erhard, M.; Fickler, R.; Krenn, M.; Zeilinger, A. Twisted photons: new quantum perspectives in high dimensions. *Light: Sci. Appl.* **2018**, *7*, 17146.
(13) Wang, J.; Liu, J.; Li, S.; Zhao, Y.; Du, J.; Zhu, L. Orbital angular momentum and beyond in free-space optical communications. *Nanophotonics* **2022**, *11*, 645−680.
(14) Forbes, A.; Ramachandran, S.; Zhan, Q. Photonic angular momentum: progress and perspectives. *Nanophotonics* **2022**, *11*, 625−631.
(15) Soskin, M. S.; Gorshkov, V. N.; Vasnetsov, M. V.; Malos, J. T.; Heckenberg, N. R. Topological charge and angular momentum of light beams carrying optical vortices. *Phys. Rev. A* **1997**, *56*, 4064−4075.
(16) Ohno, T.; Miyanishi, S. Study of surface plasmon chirality induced by Archimedes' spiral grooves. *Opt. Express* **2006**, *14*, 6285−6290.
(17) Yang, S.; Chen, W.; Nelson, R. L.; Zhan, Q. Miniature circular polarization analyzer with spiral plasmonic lens. *Opt. Lett.* **2009**, *34*, 3047−3049.
(18) Kim, H.; Park, J.; Cho, S.-W.; Lee, S.-Y.; Kang, M.; Lee, B. Synthesis and Dynamic Switching of Surface Plasmon Vortices with Plasmonic Vortex Lens. *Nano Lett.* **2010**, *10*, 529−536.
(19) Shen, Z.; Hu, Z. J.; Yuan, G. H.; Min, C. J.; Fang, H.; Yuan, X.-C. Visualizing orbital angular momentum of plasmonic vortices. *Opt. Lett.* **2012**, *37*, 4627−4629.
(20) Spektor, G.; Kilbane, D.; Mahro, A.; Frank, B.; Ristok, S.; Gal, L.; Kahl, P.; Podbiel, D.; Mathias, S.; Giessen, H.; zu Heringdorf, F.-J. M.; Orenstein, M.; Aeschlimann, M. Revealing the subfemtosecond dynamics of orbital angular momentum in nanoplasmonic vortices. *Science* **2017**, *355*, 1187−1191.
(21) Frank, B.; Kahl, P.; Podbiel, D.; Spektor, G.; Orenstein, M.; Fu, L.; Weiss, T.; Horn-von Hoegen, M.; Davis, T. J.; zu Heringdorf, F.-J. M.; Giessen, H. Short-range surface plasmonics: Localized electron emission dynamics from a 60-nm spot on an atomically flat single-crystalline gold surface. *Sci. Adv.* **2017**, *3*, No. e1700721.
(22) Zhang, H.; Zeng, J.; Lu, X.; Wang, Z.; Zhao, C.; Cai, Y. Review on fractional vortex beam. *Nanophotonics* **2022**, *11*, 241−273.
(23) Wang, Y.; Zhao, P.; Feng, X.; Xu, Y.; Liu, F.; Cui, K.; Zhang, W.; Huang, Y. Dynamically sculpturing plasmonic vortices: from integer to fractional orbital angular momentum. *Sci. Rep.* **2016**, *6*, No. 36269.
(24) Yang, Z.; Zhang, X.; Bai, C.; Wang, M. Nondiffracting light beams carrying fractional orbital angular momentum. *J. Opt. Soc. Am. A* **2018**, *35*, 452−461.
(25) Tang, B.; Zhang, B.; Ding, J. Generating a plasmonic vortex field with arbitrary topological charges and positions by meta-nanoslits. *Appl. Opt.* **2019**, *58*, 833−840.
(26) Mermin, N. D. The topological theory of defects in ordered media. *Rev. Mod. Phys.* **1979**, *51*, 591−648.
(27) Nash, C. *History of Topology*; James, I. M., Ed.; Elsevier, 1999; Chapter 12, pp 359−415.
(28) Rui, G.; Zhan, Q.; Cui, Y. Tailoring optical complex field with spiral blade plasmonic vortex lens. *Sci. Rep.* **2015**, *5*, No. 13732.
(29) Cho, S.-W.; Park, J.; Lee, S.-Y.; Kim, H.; Lee, B. Coupling of spin and angular momentum of light in plasmonic vortex. *Opt. Express* **2012**, *20*, 10083−10094.
(30) Spektor, G.; David, A.; Gjonaj, B.; Bartal, G.; Orenstein, M. Metafocusing by a Metaspiral Plasmonic Lens. *Nano Lett.* **2015**, *15*, 5739−5743.
(31) Davis, T. J.; Frank, B.; Podbiel, D.; Kahl, P.; zu Heringdorf, M. z. H.; Giessen, H. Subfemtosecond and Nanometer Plasmon Dynamics with Photoelectron Microscopy: Theory and Efficient Simulations. *ACS Photonics* **2017**, *4*, 2461−2469.
(32) Raether, H. A. *Physics of Thin Films*; Hass, G.; Francombe, M. H.; Hoffman, R. W., Eds.; Academic Press, 1977; Vol. *9*, p 145.
(33) Davis, T. J. Surface plasmon modes in multi-layer thin-films. *Opt. Commun.* **2009**, *282*, 135−140.
(34) Gorodetski, Y.; Niv, A.; Kleiner, V.; Hasman, E. Observation of the Spin-Based Plasmonic Effect in Nanoscale Structures. *Phys. Rev. Lett.* **2008**, *101*, No. 043903.
(35) Simon, D. S. *Tying Light in Knots*; Morgan & Claypool Publishers, 2018; pp 2053−2571.
(36) Bauer, T.; Davis, T. J.; Frank, B.; Dreher, P.; Janoschka, D.; Meiler, T. C.; zu Heringdorf, F.-J. M.; Kuipers, L. K.; Giessen, H. Ultrafast time dynamics of plasmonic fractional orbital angular momentum, 2023.
(37) Leach, J.; Yao, E.; Padgett, M. J. Observation of the vortex structure of a non-integer vortex beam. *New J. Phys.* **2004**, *6*, No. 71.
(38) Basistiy, I. V.; Bazhenov, V. Y.; Soskin, M. S.; Vasnetsov, M. V. Optics of light beams with screw dislocations. *Opt. Commun.* **1993**, *103*, 422−428.
(39) Jesus-Silva, A. J.; Fonseca, E. J. S.; Hickmann, J. M. Study of the birth of a vortex at Fraunhofer zone. *Opt. Lett.* **2012**, *37*, 4552−4554.
(40) Gbur, G. Fractional vortex Hilbert's Hotel. *Optica* **2016**, *3*, 222−225.
(41) Burresi, M.; Engelen, R. J. P.; Opheij, A.; van Oosten, D.; Mori, D.; Baba, T.; Kuipers, L. Observation of Polarization Singularities at the Nanoscale. *Phys. Rev. Lett.* **2009**, *102*, No. 033902.
(42) Rotenberg, N.; Spasenović, M.; Krijger, T. L.; le Feber, B.; de Abajo, F. J. G.; Kuipers, L. Plasmon Scattering from Single Subwavelength Holes. *Phys. Rev. Lett.* **2012**, *108*, No. 127402.
(43) Kabakova, I. V.; de Hoogh, A.; van der Wel, R.; Wulf, M.; le Feber, B.; Kuipers, L. Imaging of electric and magnetic fields near plasmonic nanowires. *Sci. Rep.* **2016**, *6*, No. 22665.
(44) Berry, M. V.; Liu, W. No general relation between phase vortices and orbital angular momentum. *J. Phys. A: Math. Theor.* **2022**, *55*, No. 374001.

https://doi.org/10.1021/acsphotonics.3c01024
ACS Photonics 2023, 10, 3772−3780